

Damage Areas on Selected LDEF Aluminum Surfaces*

Cassandra R. Coombs, Dale R. Atkinson, Martha K. Allbrooks,
Alan J. Watts, Corey J. Hennessy and John D. Wagner
POD Associates, Inc.
2309 Renard Place, SE
Suite 201
Albuquerque, NM 87106

ABSTRACT

With the U.S. about to embark on a new space age, the effects of the space environment on a spacecraft during its mission lifetime become more relevant. Included among these potential effects are degradation and erosion due to micrometeoroid and debris impacts, atomic oxygen and ultraviolet light exposure as well as material alteration from thermal cycling, and electron and proton exposure. This paper focuses on the effects caused by micrometeoroid and debris impacts on several LDEF aluminum plates from four different bay locations: C-12, C-10, C-01, and E-09. Each plate was coated with either a white, black or gray thermal paint. Since the plates were located at different orientations on the satellite, their responses to the hypervelocity impacts varied. Crater morphologies range from a series of craters, spall zones, domes, spaces, and rings to simple craters with little or no spall zones. In addition, each of these crater morphologies is associated with varying damage areas, which appear to be related to their respective bay locations and thus exposure angles. More than 5% of the exposed surface area examined was damaged by impact cratering and its coincident effects (*i.e.*, spallation, delamination and blow-off). Thus, results from this analysis may be significant for mission and spacecraft planners and designers.

INTRODUCTION

There is an increasing concern over the consequences of micrometeoroid and debris (M&D) impacts on space vehicles particularly due to an increasing debris population. However,

* This work was performed under subcontract to W.J. Schafer Associates, Inc., under prime contract to SDIO, contract no. SC-89W-26-11, SDIO-89-C-0034. POD Internal Project No.: 019202.

the current approach used by most satellite designers in assessing this environment produces great uncertainties in the damage estimates for certain material classes such as coated thermal control surfaces, multilayer coatings, and glasses. As the debris population grows, these uncertainties will also increase leading to more erroneous damage estimates.

The recent LDEF flight provides a unique opportunity to characterize the natural and man-made particle populations in Low-Earth Orbit (LEO) and more accurately quantify the damage areas created on a satellite which was in orbit for nearly six years. LDEF exposed 130m² of surface area to the space environment at altitudes between ~475 km (launch) - 326 km (recovery) on its 12-sided closed cylinder frame. During its tenure in space, LDEF was gravity-gradient stabilized with one end constantly facing the Earth (EARTH-end) and the opposite end constantly facing space (SPACE-end). Row 9 was constantly oriented 8° from the normal to the velocity or ram direction (RAM). This constant orientation provided a superb experimental and control platform for monitoring the effects of exposure to the LEO environment.

In this study we concentrated on the collection and evaluation of damage areas created by impact craters into thermal painted aluminum surfaces located about LDEF. These data are intended to: (1) aid in the characterization of the effects of the LEO M&D environment on satellite systems and materials, (2) update the current theoretical models for LEO, (3) help assess the survivability of spacecraft and satellites which must travel through or reside in LEO, and (4) help define future spacecraft material components.

BACKGROUND

Two major components currently exist within the dynamic LEO environment, namely natural micrometeoroids from the solar system and man-made debris dating back to the onset of space exploration in 1957. While the micrometeoroids arrive at the Earth from almost all directions, the debris is in both near-circular and elliptical orbits around the Earth. Although both types of particles exist all the way out to geosynchronous (GEO) orbits, the major populations of debris are within the altitude range of 350 - 2000 km.

Micrometeoroids arrive at the Earth with differential speeds of from below 12 km/s to 72 km/s. However, when the spacecraft orbital speed is included, the resulting impact speeds range from below 5 km/s to 79 km/s, yielding an overall average collisional speed of 20 km/s (Zook¹). The flux (number of impacts per area per time) of particles is approximately isotropic in free space as seen from the Earth, but the effect of Earth shielding causes an asymmetry as seen by an orbiting spacecraft in LEO, resulting in a minimum number of impacts for Earth-facing satellite surfaces. As a result, either the RAM surface or the SPACE-facing surfaces (depending upon altitude) receive the highest number of impacts (Atkinson, *et al.*²).

Debris population distribution is largely a function of launch frequencies and sites with subsequent perturbations caused by accidental (and/or deliberate) explosions, collisions, fragmentations, surface erosion, and manned or unmanned mission-related debris (*e.g.* ejected lens covers, explosive bolts). Currently, the greatest concentration of debris occurs at inclinations toward the pole, with peaks at 60°, 80°, and 100° (Kessler³). Once created, differential precessions will cause the initial "clouds" of space debris to form a toroid, or belt, around the Earth with holes near the pole. Consequently, the flux of particle impacts on a spacecraft is a function of the latter's inclination and also altitude, and the resulting impact speeds can range from zero to about 16 km/s for near-circular orbits (or to about 19 km/s for highly elliptical debris orbits such as Hohman transfer orbits out to GEO).

For both micrometeoroids and debris, the particles can range in size from sub-microns to many centimeters. However, both components display a power law of number versus size, with the smaller particles being far more numerous than the larger ones. While particles greater than 1 mm can penetrate typical satellite skins and cause catastrophic damage, the smaller particles mostly cause a gradual degradation of a satellite's surfaces, including thermal control paints, thermal blankets, coatings to provide protection against atomic oxygen (AO) or ultraviolet light (UV), solar cells and optics. Many satellite surfaces employ coatings which range from sub-micron (*e.g.*, optics) to mils (*e.g.*, thermal control, AO and UV protection, and solar cell covers). At impact speeds of 5 - 20 km/s particles can penetrate materials (either punching holes or causing craters with associated radial (star) cracks for brittle materials), and can cause damage

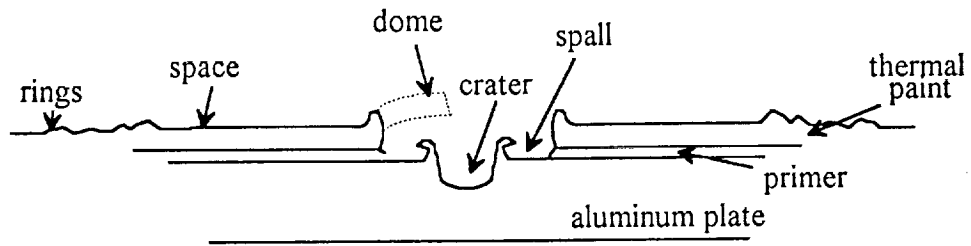
regions which are considerably larger than the incoming particle. Consequently, the thermal paint coatings can be locally disrupted even by particles as small as 1 to 100 μm , and the areal number density (hits per square meter) can easily exceed 1000/ m^2 for a multi-year mission.

When a hypervelocity particle impacts a surface it either creates a crater or perforates the surface (also referred to as the target). In addition to crater formation, surrounding areas can experience spallation, cracking or delamination of an attached layer as depicted in Figures 1a and 1b. These damage effects can lead to reduced structural strength, thermal and optical property degradation and erosion of underlying materials. The physical response of any target to an M&D impact depends on the material, induced stress level, material temperature, number of projectiles and the system configuration. These phenomena may be enhanced by subsequent exposure of underlying layers to the UV, atomic oxygen, charged particles, and thermal cycling. This subsequent exposure can modify a material and thus enhance cracking and delamination regions. Also, material embrittlement, erosion and other property degradation can occur to either the surface or exposed underlying material. For example, AO can creep under locally delaminated regions causing greater damage, or previously protected materials may become exposed to UV through small cracks or fissures. In short, the synergistic environment can lead to accelerated damage rates and a significant increase in the damage zone.

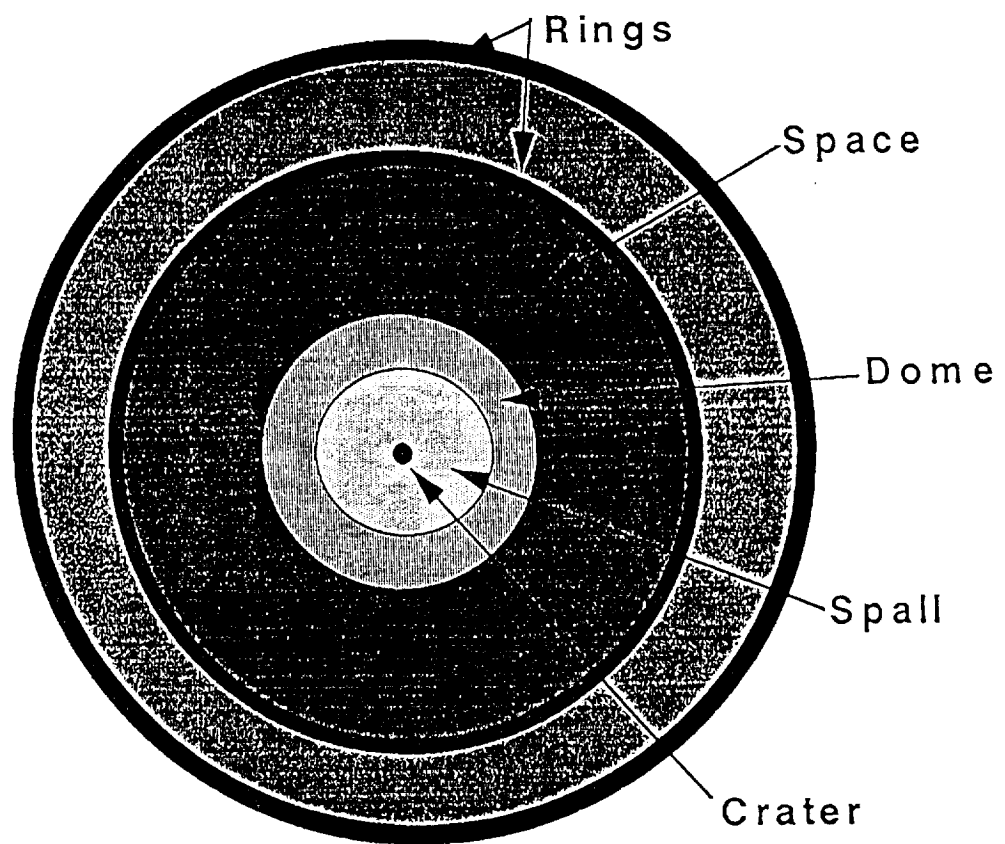
DATA COLLECTION

Impact craters were analyzed on three leading edge components (C-10 EOOB, Active Grapple; C-12 EOOA, Experiment S0109; and E-09 E00A, E00B, E00C, and E00D, Experiment S0014) and one trailing edge component (C-01 EOOB, Inactive Grapple). These materials were composed of anodized aluminum and coated with either black or white Chemglaze thermal control paints. Each plate is discussed more completely below.

The crater measurements were taken at the NASA Johnson Space Center Facility for Optical Investigation of Large Surfaces (FOILS) Laboratory. This facility is a Class 100 clean room designed specifically for analyzing space hardware. The scanning apparatus consists of a



(a)



(b)

Figures 1a and 1b: (1a) Schematic cross-section of a "typical" impact into a thermal painted aluminum plate on LDEF. (1b) Plan view of a "typical" crater on LDEF, corresponding to the cross-section in 1a.

binocular microscope attached to a scanning table along with computer operated data collection and monitoring system. Once measured, each crater was catalogued and became part of the Meteoroid and Debris Special Investigation Group (M&D SIG) database.

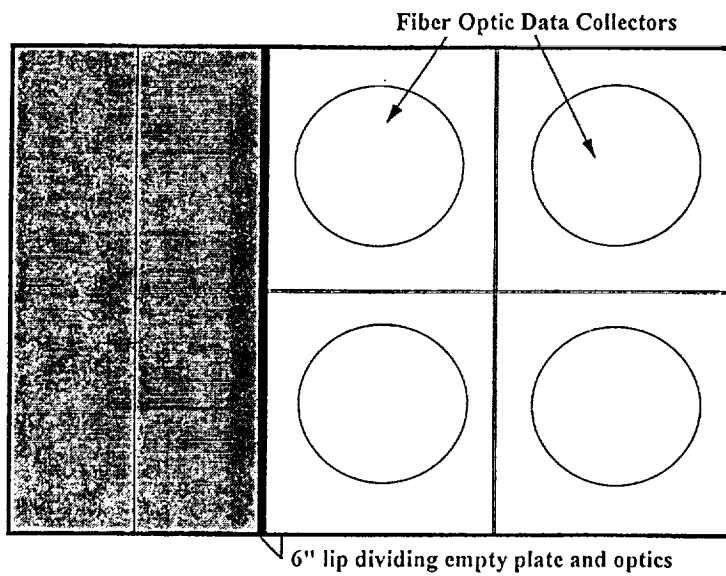
Before crater measurement began on the LDEF hardware, a cursory analysis was made of the surface of the component and a decision was made to only measure those craters larger than 75 microns as these could be consistently identified. All craters smaller than this that could be discerned were counted and recorded. For measurement and logistic purposes, individual impact zones were divided, or categorized, into five different morphologic features (Figures 1a and 1b). These include: crater, spall, dome, space, and ring. Individual measurements, in microns, were made of crater, spall, dome and ring radii at the four "clock" positions, 3, 6, 9 and 12.

Virtually all features which measured greater than 0.2 mm in size possessed a spall zone in which all of the paint was removed from the aluminum surface immediately adjacent to the crater. These spall zones varied in size from approximately 2 - 5 crater diameters. The actual craters in the aluminum substrate varied from central pits without raised rims, to morphologies more typical of craters formed in aluminum under hypervelocity laboratory conditions. Most features also possessed what is referred to as a "shock zone"¹ as well. These zones varied in size from approximately 1 - 20 crater diameters. In most cases, only the outer-most layer of paint was affected by this impact related phenomenon. Several impacts exhibited ridge-like structures ringing the area in which this outer-most paint layer was removed. There was only one noticeable perforation and associated backside spallation feature, which was on component E-09 E00D. All other trays showed no evidence of such phenomena.

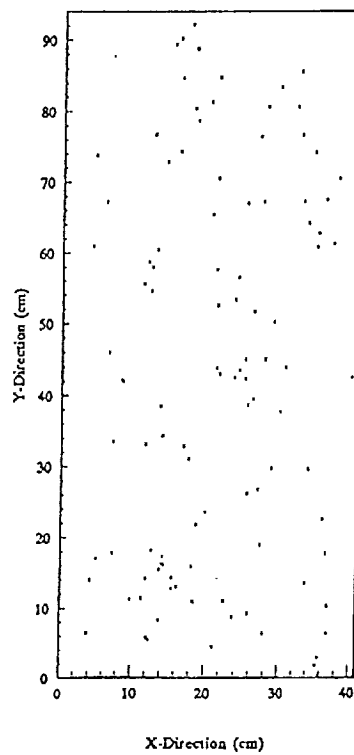
LDEF Components Measured

Bay C-12

The C-12 plate examined was a Chemglaze A278 white-painted aluminum electronics coverplate that occupied the left third of the C-12 experiment tray (Figure 2a). Bay C-12 was located approximately 82° from RAM. Figure 2b shows the distribution of impacts on this painted aluminum plate.



(a)



(b)

Figure 2a and 2b: (2a) Schematic diagram of the relationship between the C-12 aluminum plate and the S0109 experiment. (2b) Schematic diagram of LDEF aluminum plate from Bay C-12. Small dots represent locations of impacts measured on this plate.

Bays C-10 and C-01

Bay C-10 was occupied by one of two grapple fixtures aboard the spacecraft. This particular grapple fixture was the active grapple located toward the leading edge, approximately 22° from RAM, and was used to give the initiate signal through the LDEF initiation system to the Experiment Power and Data Systems (EPDS). The grapple fixture was attached via a base (abutment) plate to a 3.2 mm thick 6061-T6 anodized aluminum plate which resided in the bottom of the tray. Next to the grapple fixture was a small array of light emitting diodes (LEDs), which were used to show the active status of the LDEF spacecraft. These were mounted in a black painted aluminum plate which was mounted flush with the bottom of the grapple tray. Each grapple fixture consisted of an aluminum grapple pin, three brushed aluminum spindles to which the Shuttle Remote Manipulator System (RMS) could attach itself, and an alignment target for the RMS operator to use when grappling the spacecraft.⁴ A small (approx. 1" dia.) Teflon button was located at the end of each grapple pin. During deintegration of the satellite, the grapple fixtures were dismantled completely. Thus, during this study, only the abutment plate sections of these grapple fixtures were examined. Figure 3 shows the distribution of impacts on the C-10 abutment plate. The C-01 grapple fixture was totally passive and was used exclusively for the deployment and retrieval of the LDEF spacecraft. This grapple fixture was located toward the trailing edge of LDEF, at 112° from RAM. Figure 4 shows the distribution of impacts on the C-01 abutment plate.

Bay E-09

Housed in Bay E-09 was an active experiment tray (Figure 5a) which contained experiment S0014, the Advanced Photovoltaic Experiment.⁵ This tray was oriented approximately 8° from RAM. Specific objectives of this experiment were to provide information on the performance and endurance of advanced and conventional solar cells, to improve reference standards for photovoltaic measurements, and to measure the energy distribution in the extraterrestrial solar spectrum.

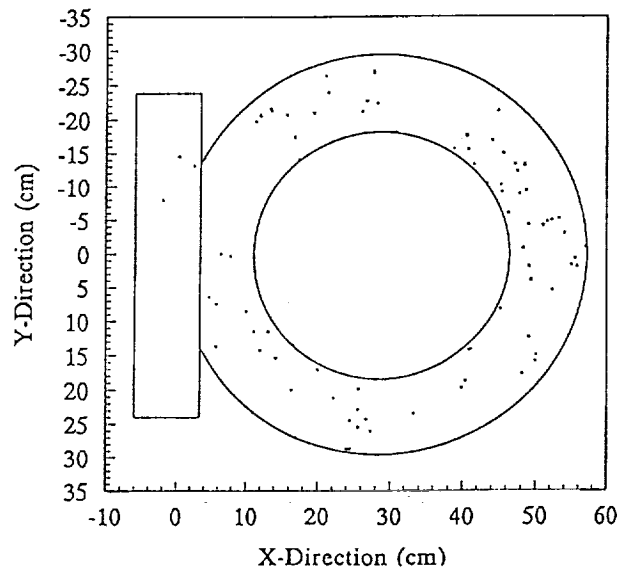


Figure 3: Schematic diagram of the active grapple abutment plate from Bay C-10. The small dots represent the locations of the craters measured in this study.

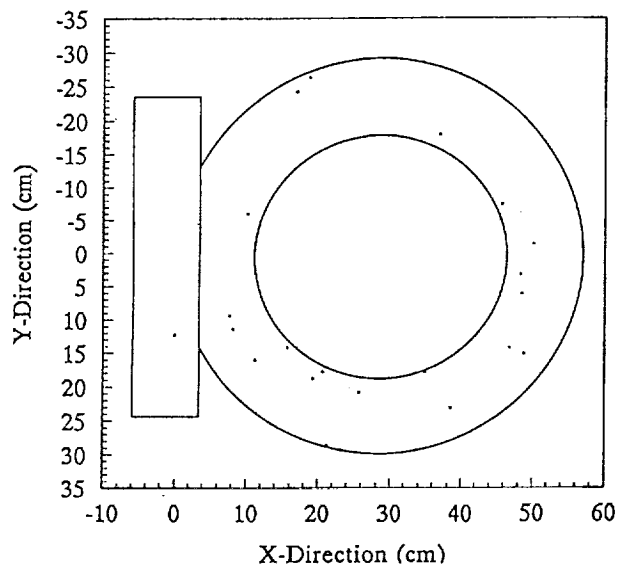
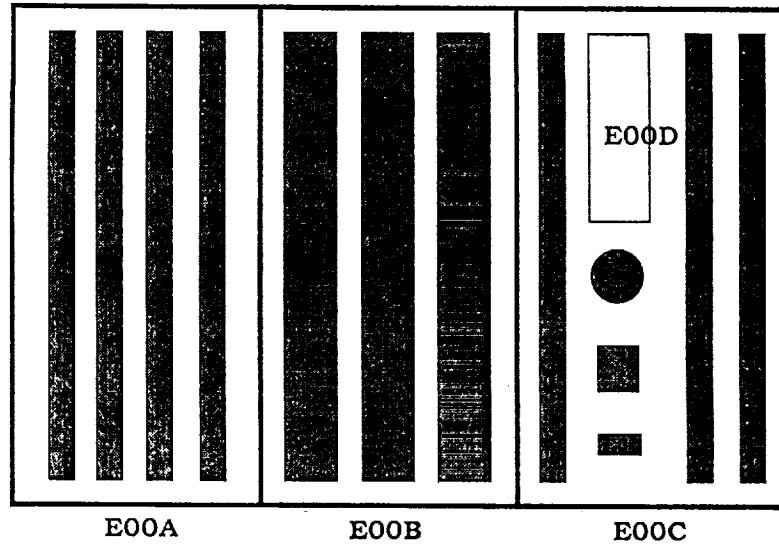
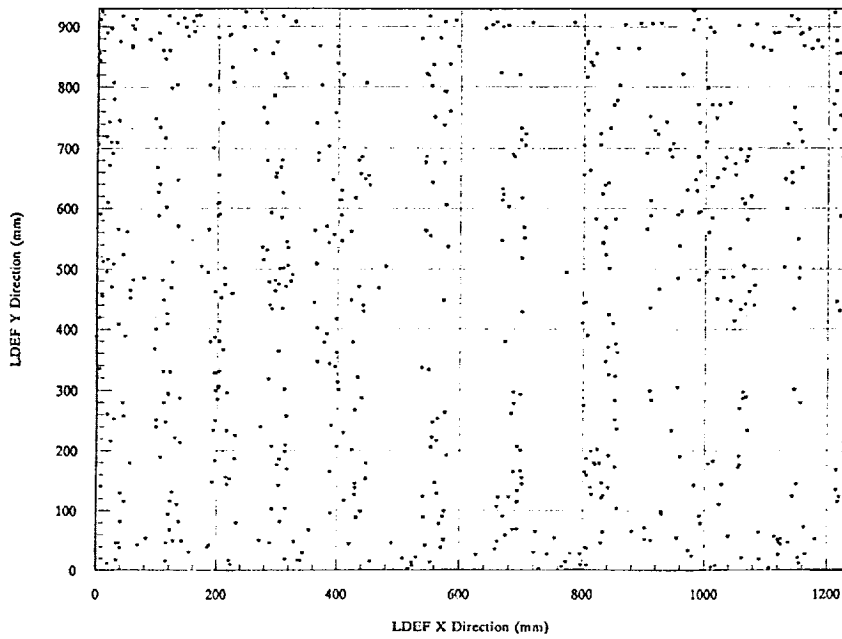


Figure 4: Schematic diagram of the inactive grapple plate from Bay C-01. The small dots indicate the locations of the craters measured in this study.



(a)



(b)

Figures 5a and 5b: (5a) Schematic diagram of the aluminum plates measured from Bay E-09. (5b) Schematic diagram of the distribution of impact craters on these plates. The small dots indicate the locations of the craters measured in this study.

The 12 inch-deep experiment tray used two LiSO₂ batteries to run the Experiment Power and Data System Collection. The hardware onboard consisted of numerous silicon and gallium arsenide solar cells, solar cell covers, and solar cell modules and assemblies. The experiment also contained a series of optical bandpass filters with multiple layers of materials such as aluminum, magnesium fluoride, silicon dioxide, silver, thorium fluoride, zinc sulfide, lead fluoride, and cryolite. Optical materials and substrates were composed of a variety of fused silica, Corning, and Schott glasses. Each of the experiment samples was mounted under a slotted, Chemglaze Z306 black thermal control painted 6061-T6 aluminum frame. The ~1.6 inch thick aluminum plates were intended to limit the field of view of the solar cells and other hardware. Figure 5b shows the distribution of impacts on these aluminum plates.

RESULTS

Results from the crater measurements taken in this study are summarized in Table I and discussed below.

Bay C-12

There were more than 250 impact features measured on this tray with an average damage area of $1.1 \times 10^8 \mu\text{m}^2$. The largest crater was 0.95 mm in size, and the total average damage area for this leading edge plate was 3.14%.

As described above, a paint spall zone was commonly found in association with the central pit or crater in most of the impacts examined from this tray. Around this spall zone was a smooth area (*e.g.*, "space", Figure 1) varying in size from five to 10 crater diameters. One or more rings were typically found outside this smooth region. Several of the more notable rings appear as "fold-over" flaps (or wrinkles) in the paint, while the remainder of the rings appear as powdery ripples (*e.g.*, powdered remnants) as seen in Figures 6, 7, 8 and 9.

Table 1: LDEF Damage Area Data on Selected Aluminum Panels

LDEF Aluminum Plate	Number Impacts Observed	Total Damage Area	Average Damage Area (μm^2)	Mean Crater Diameter (μm)	Mean Spall Diameter (μm)	Number Impacts per cm^2
C-12	253	3.14 %	1.09×10^8	322.5	658.9	0.07
C-10	94	2.09 %	4.36×10^7	299	696.0	0.05
C-01	30	0.26 %	1.88×10^7	316.5	877.1	0.01
E-09	521	0.32 %	3.034×10^5	185	208.5	0.11

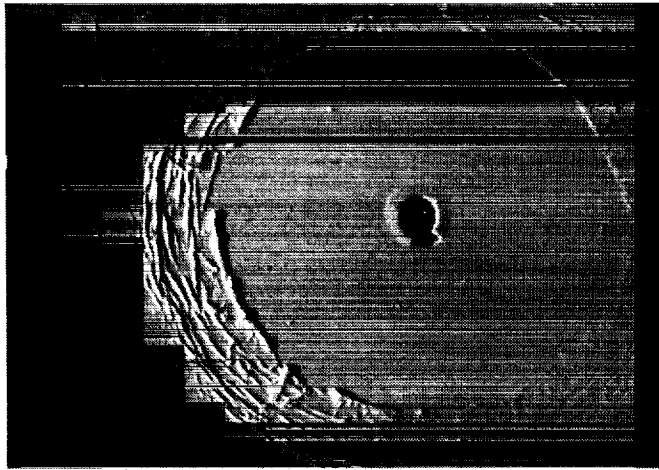


Figure 6: Impact crater from Bay C-12 showing crater, spall, dome, space, and rings. This crater is considered "young" as described in the text. Crater diameter $\sim 200 \mu\text{m}$, outer ring diameter $\sim 11 \text{ mm}$; magnified 12x.

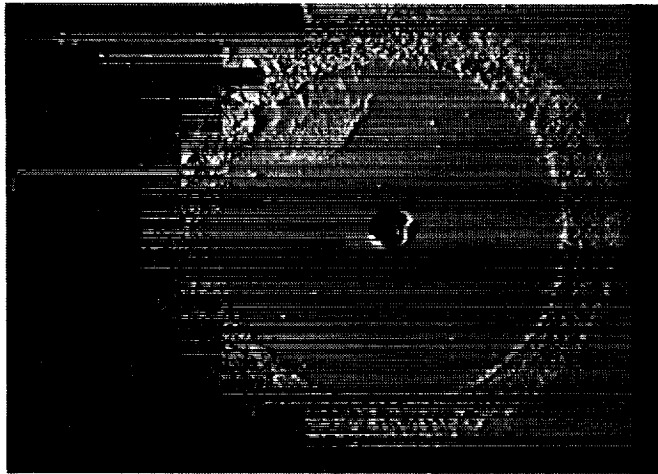


Figure 7: "Middle" age impact crater from Bay C-12 as discussed in text. "Blob" at eleven o'clock center is ejecta from central crater. Crater diameter $\sim 350 \mu\text{m}$, outer ring diameter $\sim 15 \text{ mm}$; magnified 8x.

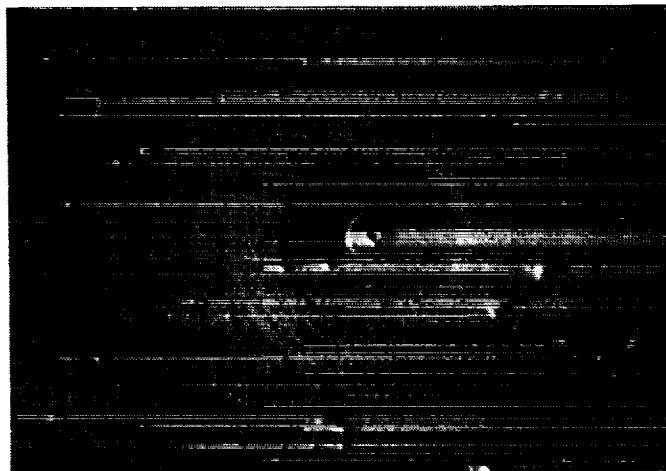


Figure 8: "Old" impact crater from Bay C-12 as discussed in text. Crater diameter $\sim 90 \mu\text{m}$, outer ring diameter $\sim 4.5 \text{ mm}$; magnified 18x.

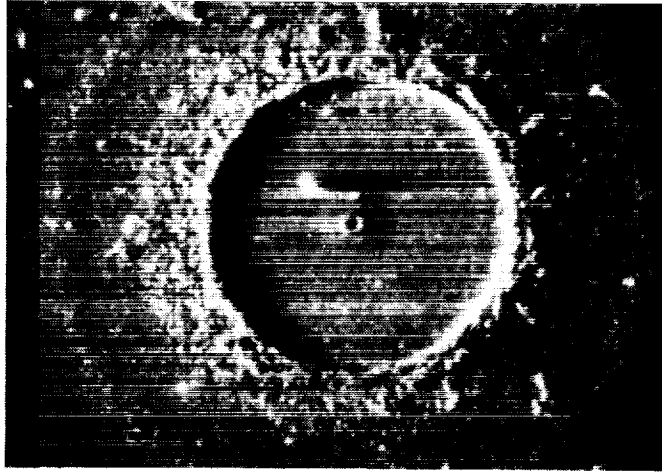


Figure 9: Impact crater from Bay C-12 showing fine powderiness of ring structure and paint surface. Crater diameter is $35\ \mu\text{m}$, total ring diameter is $\sim 1.6\ \text{mm}$; magnified 40x.



Figure 10: Typical impact crater from Bay C-10 showing crater, spall and domed regions. Crater diameter is $\sim 85\ \mu\text{m}$; magnified 50x.

Bays C-10 and C-01

We documented a total of 94 craters on C-10, and 30 on C-01. This corresponds to approximately one impact crater per 19 cm² for C-10, and one impact crater per 72 cm² for C-01. The craters ranged in size from 0.45 mm to 1.53 mm with an average damage area of $5 \times 10^7 \mu\text{m}^2$ for C-10 and $2.1 \times 10^7 \mu\text{m}^2$ for C-01. These craters are typical of craters produced in aluminum during laboratory hypervelocity impact tests. Impacts into the painted surfaces of the grapple fixture caused front surface spallation, and the craters were sometimes surrounded by minor spall zones, small domes, and rings (Figure 10).

Bay E-09

More than 520 craters were measured on the four components of E-09, yielding approximately one impact per 94 cm². The average damage area for these craters was $3.4 \times 10^5 \mu\text{m}^2$, with a mean crater diameter of 185 μm .

These craters typically did not exhibit multiple ring structures, nor were large "spaces" observed. For the most part, the morphologies of these craters consisted of a central impact crater with minor spall and/or doming. This data from Bay E-09 is difficult to assess since the black thermal control paint had been almost entirely eroded, leaving behind only the primer coat. Space weathering and erosion probably removed all vestiges of the rings, as well as many of the other impact features.

Statistical Analyses

Crater diameter was compared to spall diameter, dome diameter, ring diameter, space diameter, and total damage zone using statistical techniques to attempt to find simple math models which would correlate damage effects per impact. The statistical analysis tools in the commercial software packages *Superbase*⁶, *GrafTool*⁷, and *Matlab*⁸ were employed in this effort.

The models developed in this analysis are acceptable first-order models of the damage effects on these components *within the bounds of the actual data*. It is always hazardous to extrapolate best-fit curves beyond the bounds of the data, and particularly so if the leading

coefficient is negative. This is because the negative leading coefficient implies a decreasing (for example) spall diameter for large crater diameters, which will eventually yield a zero spall diameter for large crater diameters, and a negative spall diameter for some very large crater diameter. The idea of a negative spall diameter is clearly nonsense, so these, like all simple models, should be regarded as valid only within the bounds specified.

In conducting this analysis, we assumed that all data fit a Poissonian distribution which collapses into a Gaussian distribution for large numbers and applied the tools that would be appropriate for such a distribution. While not strictly correct, the errors introduced by this particular approximation are probably not large. Further, the data sets analyzed were of such small size that all results should be regarded as indicators of trends, and not as absolute answers. It is generally accepted that Gaussian statistics only begin to be valid at sample populations of 30 or more, and that populations on the order of 1000 or more are required to establish an answer with any confidence. Few of our data sets had 30 or more samples, and none had anywhere near 1000. Limited data sets are an inherent problem in field collection of random-event phenomena, and, as a result, one is forced to live with a less-than-perfect analysis.

The first effect examined was spall formation as a function of crater diameter. The best-fit curve for the data in all cases was a second order polynomial, yielding an equation of the form

$$y = ax^2 + bx + c \quad (1)$$

where y is the variable (*i.e.*, spall, dome, space, ring or damage zone) diameter and x is the crater diameter and a , b , and c are constants. The second effect analyzed was dome formation as a function of crater diameter, followed by the relationship between ring and crater diameters, space and crater diameters, and lastly the total damage zone versus crater diameter. Regression coefficients for each curve were calculated, along with their squares, also sometimes referred to as the "goodness-of-fit" parameter. Math models are generally considered acceptable if the square of the correlation coefficient is 0.50 or greater. These condensed data are shown in Table 2.

Table 2: Statistical Data from Selected LDEF Aluminum Panels

LDEF Bay Location	Component ID	Spall vs. Crater		Dome vs. Crater		Space Vs. Crater		Ring vs. Crater		Total Damage Area vs. Crater	
		r*	r ² *	r	r ²	r	r ²	r	r ²	r	r ²
C-12	E00A	0.92	0.85	0.53	0.29	0.6	0.36	0.65	0.42	0.69	0.49
C-10	E00B	0.88	0.77	0.58	0.33	0.65	0.43	0.91	0.83	0.67	0.45
C-01	E00B	0.91	0.82	0.93	0.87	NA	NA	NA	NA	0.91	0.82
E-09	E00D	0.88	0.78	0.5	0.25	NA	NA	0.77	0.59	0.76	0.58

*r = correlation coefficient from best fit curve

r² = square of correlation coefficient; number > 0.5 indicates a good math fit

The best fits were found for the spall and dome comparisons. This might be expected, since both spallation and dome formation happen immediately upon impact, and are localized to the impact point. The space and ring phenomena are probably sensitive to such factors as local thickness of paint and the degree of embrittlement or erosion or changes in mechanical properties (e.g., modulus or strength). Thus these other effects of interest yielded much less satisfactory correlations.

The four plots shown in Figures 11a through 11d include comparisons of average crater diameters to average spall, dome, space, and ring diameters in the 3-9 and 6-12 clock positions. These figures also illustrate the variation in regression curves for the LDEF aluminum plates measured. These fits are reasonable but not great.

SUMMARY AND DISCUSSION

The three leading edge sections, C-12, C-10 and E-09, have undergone a considerable amount of atomic oxygen erosion as they were facing in the RAM (velocity) direction. As such, the paint surfaces have been etched and pitted. The rough texture is produced as a result of the organic binder in the paint being sputtered away upon contact with the atomic oxygen while the paint pigment particles are left behind. A distinct difference in degree of space weathering was noticed between the grapple plates (C-10 and C-01) which, as mentioned above, faced opposite directions. Both were painted with a gray colored thermal control paint prior to launch. While the initial gray paint surface on the leading edge plate (C-10) was weathered to a rough grayish-white color, the trailing edge plate (C-01) turned a darker grayish-brown due to UV darkening of the organic paint binder. In addition, the impacts into the C-10 plate produced larger damage areas relative to crater size as compared to those in C-01.

Three "types" of ringed impact features were identified and loosely characterized as "young", "middle", or "old". This is an indication of their possible relative sequence of formation (Figures 6, 7, and 8 respectively). Preliminary analyses suggest that the different characteristics may signify a difference in relative ages between the three types of impact features. Type one, or

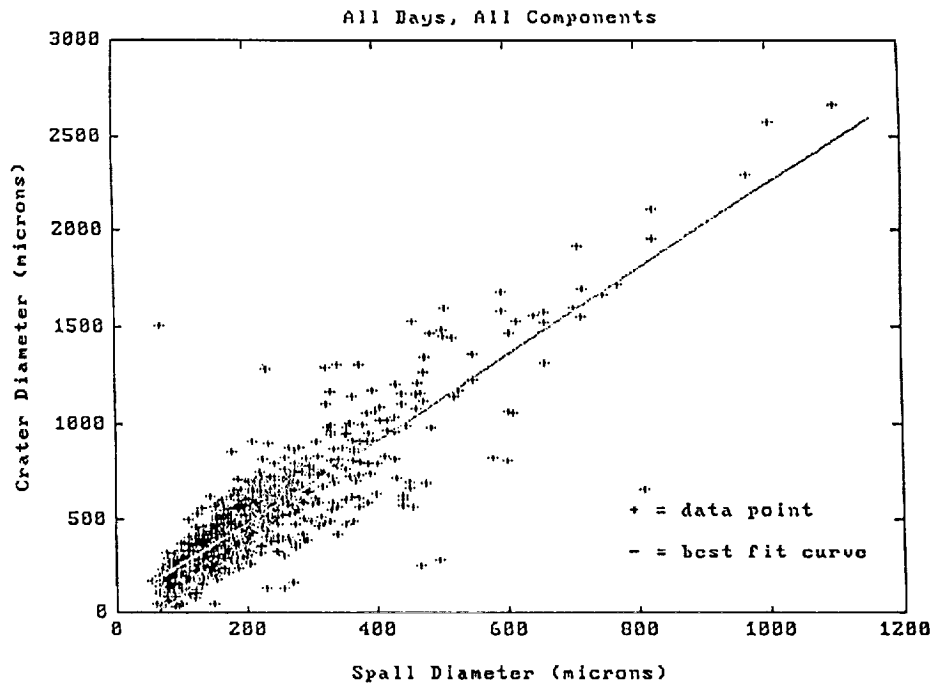


Figure 11a: Comparison plot of crater diameter versus spall diameter for all four components measured in this study.

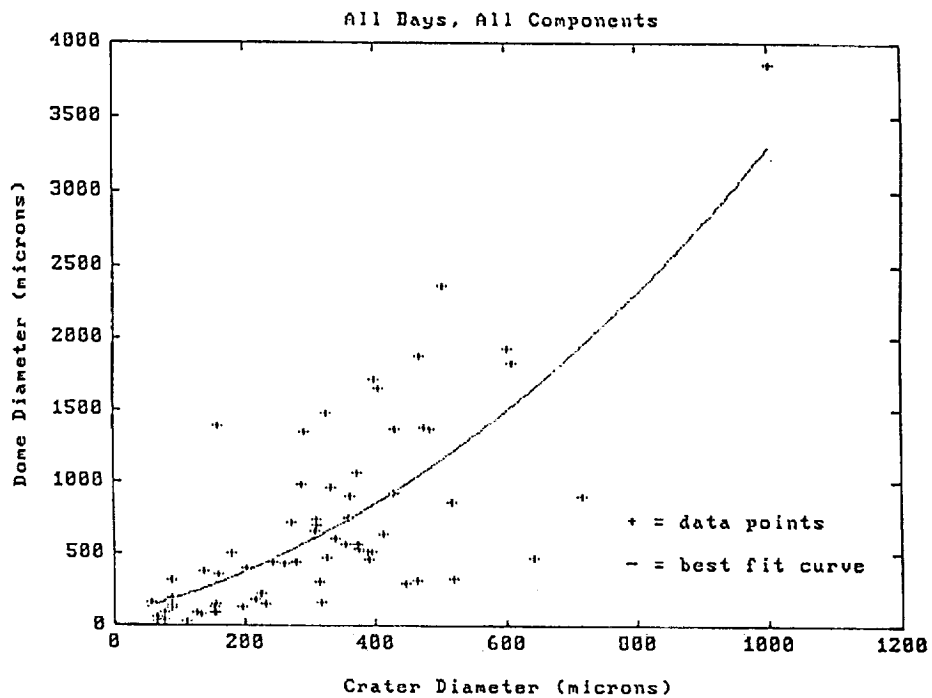


Figure 11b: Comparison plot of crater diameter versus dome diameter for all four components measured in this study.

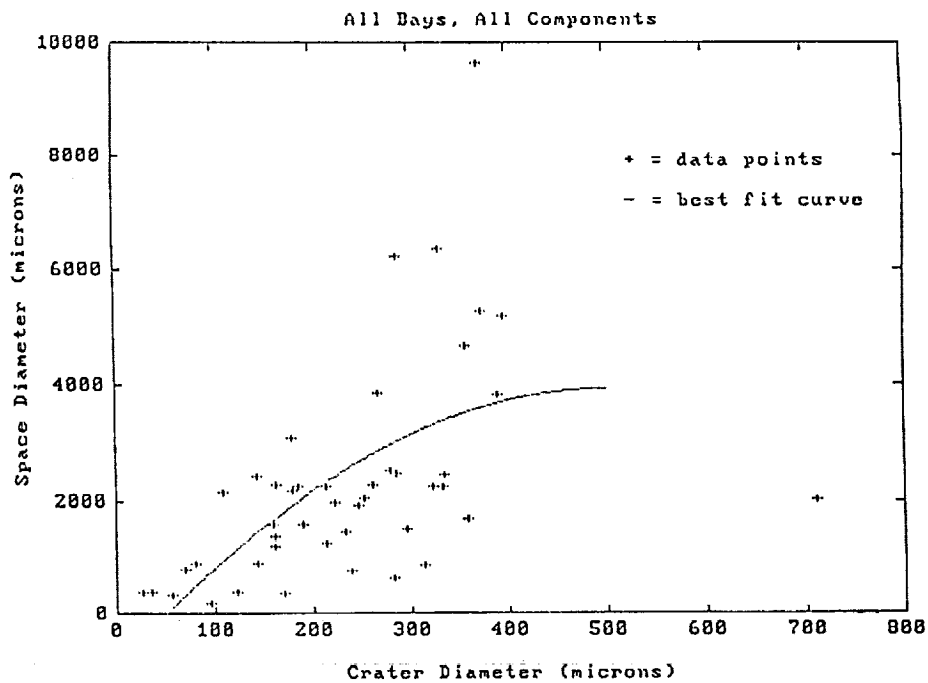


Figure 11c: Comparison plot of crater diameter versus space diameter for all four components measured in this study.

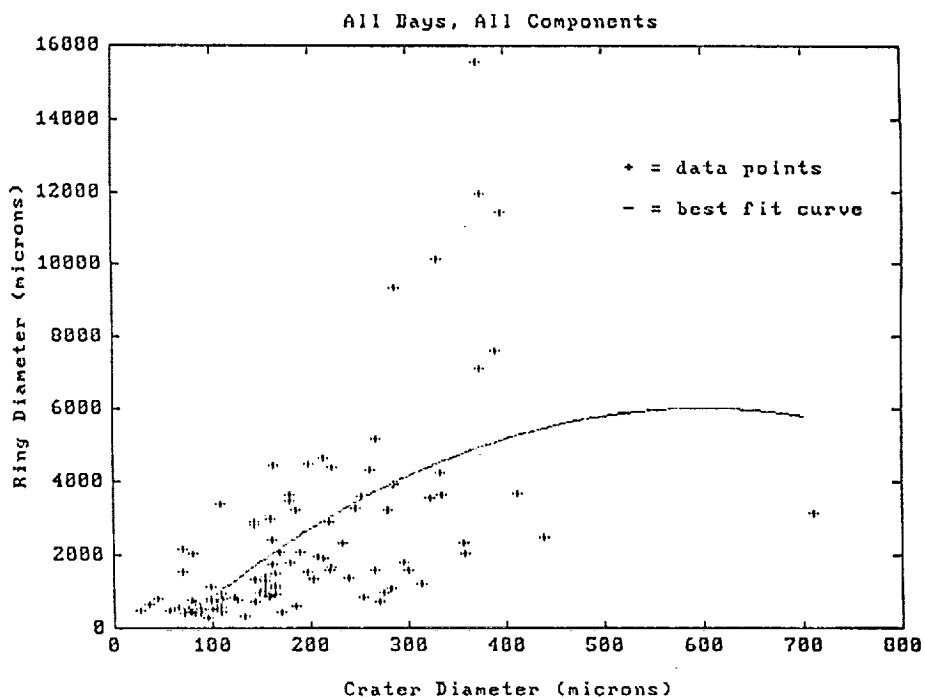


Figure 11d: Comparison plot of crater diameter versus ring diameter for all four components measured in this study.

the "young" group are characterized by very distinct crater lips, and excavation cavity rims where distinct, visible "flaps" or folds compose the ring zone (Figure 6). In these impact features, it appears as if the shock from the impact separated a layer or two of paint from the substrate and caused it to curl and fold back on itself, much as if one were scraping old paint from a wall. The impact feature as a whole is very clean and fresh. The second, or "middle" stage, appears slightly degraded. The ring edges are still distinct and some trace of the folded over layers may still be seen. In general, however, the impact feature is less obvious, and the rings appear to be rougher (Figure 7). In the third, or "old" stage, the impact feature is noticeably eroded. Little or no trace of the foldover flaps are visible and the rings have degraded into masses of rubble that appear as if they were deposited on the surface. No indications of layer fold-back are present (Figure 8).

Following discussions with Dr. Bruce Banks⁹ of NASA Lewis Research Center, we conclude that these effects are predominantly due to AO weathering along with some synergistic effects from the rest of the space environment (*e.g.*, UV embrittlement, thermal cycling). While we had initially thought that the rough, worn-down edges of these rings were due to AO weathering of the paint following impact, we now believe that the surface has been AO weathered considerably prior to impact and thus created the "powdery" effect. The spaces and rings associated with some of the craters are most likely created by Rayleigh wave propagation through the loosely adhered pigment particles on the surface, combined with interference shock waves reflecting from the front and rear surfaces of the paint and aluminum. The greater the powderiness, the more AO weathering the surface experienced prior to impact. We still cannot, however, predict the ages of these craters and features, only the relative time frame in which they occurred: *i.e.*, the more pronounced rings occurred early in LDEF's exposure, while the most powdery rings occurred much later in LDEF's exposure history, after the AO had degraded the thermal paint surface. Therefore, "age" refers to the status of the target surface *prior* to impact.

Damage Area vs. Impact size

Estimation of damage areas and combined effects degradation can produce dramatically different results than simply predicting crater size or surface degradation due to the M&D

environment alone. Typical effects found in targets impacted by space debris include surface spallation, fracture zones and delamination from the interface layer as presented and discussed above. Once cracks or openings form they provide stress concentration centers for thermal induced lateral stresses as well as entry points for AO, UV, electrons, protons and so on. Depending on the intensity and timing of this loading it is likely that continued crack propagation and/or delamination will continue into the subsurface material(s). The level of degradation and increased damage will depend on the length of impact generated cracks or delaminations and the amount of exposure to the external elements.

Data from LDEF indicates that damage areas associated with an individual impact are much larger than the initial crater or penetration area. This is illustrated by the data in Table 3. Here, degradation data from C-10 (a gray thermal painted aluminum plate), C-12 (a white thermal control coated aluminum plate), and E-09 (a black thermal control coated aluminum plate) were combined and averaged over all satellite locations. For example, for the white thermal control paint, the ring diameter ratios ranged from 5 to a maximum of 40 with an average ring diameter ratio of 17.4.

Table 3. Damage Area Ratios on LDEF

Damage Region Description	Mean Diameter Ratio (Total Damage Diameter /Crater Diameter)	Mean Area Ratio
Spall	3	5
Dome	5	7
Space	8	78
Ring	13	279

Caution is advised, however, when estimating total damage areas for a spacecraft in a given scenario. Although this LDEF example illustrates the potential severity of the problem, the LDEF orbit was relatively benign with respect to impacts. Also, virtually no data exists on the damage areas for the different materials being used by satellite designers. Due to this lack of data,

estimates of degradation from the M&D environment may be erroneously small as shown in this discussion. Therefore, while a first estimate may be based on the assumption that a small particle will merely penetrate the coating surface and the resulting damage area will also be small, the combined effects may show the damaged area to be substantial. Also, the total number of impacts will increase with mission length, and should be considered a non-linear function due to the steady escalation of the man-made debris population. Hence, future satellites could suffer greater areas of damage due to M&D induced degradation or perforation.

Recommended Approach for Assessing Damage Zones

The following outlines an approach to obtaining the needed data for estimating damage zones for spacecraft materials. This information will essentially supply the missing data and theoretical developments to the "Meteoroid Damage Assessment" report written by V.C. Frost (1970).¹⁰

- 1) Identify different material classes and any thin coatings for estimating damage zones. Material classes would include metals, composites, ceramics (*i.e.*, glasses, paints and structures), refractories, inorganic and organic plastics. Single layer materials should be considered separately from multi-layered ones.
- 2) Obtain multiple samples of each type for inclusion in test program.
- 3) Select facility(ies) which produce particles with a range of mass and velocities for micrometeoroid and debris in a controlled, accurate and reliable fashion.
- 4) Pre- and post-characterize all samples for relevant performance properties (*i.e.*, optical, thermal, and mechanical).
- 5) Identify samples and facilities for testing combined environmental effects. For example, damage areas for an alumina coated silver mirror sample will change upon exposure to an M&D environment, which may make the underlying silver layer susceptible to atomic oxygen erosion.
- 6) Develop empirical fits to data as a function of material class, environment(s), and configuration (*i.e.*, layers).
- 7) Develop damage models as a function of the same variables in (6) which can be imported into existing hydrodynamic codes in order to predict response.

- 8) Benchmark hydrodynamic code(s) against experimental data.

These data will allow theoretical and empirical formulations to be developed to predict damage zones which will better quantify expected damage and degradation suffered during a mission due to the synergistic space environment.

REFERENCES

- (1) Zook H.A. : Meteoroid Directionality on LDEF and Asteroidal Cometary Surfaces (abstract). *In Lunar and Planet. Sci. Conf. XXII*, Lunar and Planetary Institute, Houston, TX, pp. 1385-1386, 1990.
- (2) Atkinson D.A.; Watts A.J.; Crowell L.: *Final Report: Spacecraft Microparticle Impact Flux Definition*. Prepared for: LLNL, Univ. of Calif. by POD Associates, Inc., 1991.
- (3) Kessler D.J.; Reynolds R.C.; Anz-Meador P.D.: Orbital Debris Environment for Spacecraft Designed to Operate in Low Earth Orbit. *NASA TM-100471*, 1988. See also D.J. Kessler, Orbital Technical Interchange Meeting, Phillips Laboratory presentation, 2-3 April, 1991.
- (4) See T.H.; Allbrooks M.K.; Atkinson D.R.; Simon C.; and Zolensky M.: Meteoroid and Debris Impact Features on the Long Duration Exposure Facility: A Preliminary Report. *NASA JSC #24608*, 1990.
- (5) Clark L.G.; Kinard W.H.; Carter D.J. Jr.; Jones J.L. Jr., eds.: The Long Duration Exposure Facility (LDEF): Mission 1 Experiments, *NASA SP-473*, 1990.
- (6) *Superbase*, Precision Inc., Irving, TX, 1990.
- (7) *GrafTool*, 3-D Visions Corporation, Redondo Beach, CA, 1990.
- (8) *Matlab*, The Math Works Corporation, Worchester, MA, 1989.
- (9) Banks, B.: Personal Communication, 1991.
- (10) Frost V.C.: Meteoroid Damage Assessment. *NASA SP-8042*, 1970.